Journal Pre-proofs

Research paper

Influence of oxygen deficiency on optical and dielectric properties of $La_{0.75}Ba_{0.10}Sr_{0.15}FeO_{2.875-}$ compounds

M. Bouzayen, R. Dhahri, A. Benali, S. Chaabouni, K. Khirouni, B.F.O. Costa

PII: S0009-2614(20)30021-X
DOI: https://doi.org/10.1016/j.cplett.2020.137106
Reference: CPLETT 137106

To appear in: *Chemical Physics Letters*

Received Date: 27 November 2019
Revised Date: 8 January 2020
Accepted Date: 9 January 2020

Please cite this article as: M. Bouzayen, R. Dhahri, A. Benali, S. Chaabouni, K. Khirouni, B.F.O. Costa, Influence of oxygen deficiency on optical and dielectric properties of $La_{0.75}Ba_{0.10}Sr_{0.15}FeO_{2.875-}$ compounds, *Chemical Physics Letters* (2020), doi: https://doi.org/10.1016/j.cplett.2020.137106

Influence of oxygen deficiency on optical and dielectric properties of $La_{0.75}Ba_{0.10}Sr_{0.15}FeO_{2.875-\delta}$ compounds

M. Bouzayen[a], R. Dhahri[b], A. Benali[b,d], S. Chaabouni[a], K. Khirouni[c], and B. F.O. Costa[e]

[a] Laboratoire des Sciences des Matériaux et d'environnement, Faculté des Sciences de Sfax, Université de Sfax, B.P. 1171, 3000 Sfax, Tunisia

[b] Laboratoire de Physique Appliquée, Faculté des Sciences de Sfax, Université de Sfax, B.P. 1171, 3000 Sfax, Tunisia

[c] Laboratoire de Physique des Matériaux et des Nanomatériaux Appliquée à L'environnement, Faculté des Sciences de Gabes Cite Erriadh, Université de Gabes, 6079 Gabes, Tunisia

[d] I3N and Physics Department, University of Aveiro, 3810-193 Aveiro, Portugal

[e] CFisUC, Physics Department, University of Coimbra, Rua Larga, P-3004-516 Coimbra, Portugal

Abstract:

Using the conventional sol-gel process, the series of non-stoichiometric oxygen lanthanum ferrites with the formula $La_{0.75}Ba_{0.10}Sr_{0.15}FeO_{2.875-\delta}$(δ=0.00, 0.125 and 0.25) were prepared. X-ray diffraction analysis confirmed the formation of the orthorhombic structure with Pnma space group. In the present work, we confirm the potential of $La_{0.75}Ba_{0.10}Sr_{0.15}FeO_{2.875-\delta}$(δ=0.00, 0.125 and 0.25) as an efficient dielectric material. All samples show high absorbance in the visible region with wavelength above 300 nm. The optical band gaps are found to increase from 3.25 to 4.1 with increasing oxygen vacancy concentration. The dielectric constant, dielectric loss and loss factor were carried out as a function of oxygen vacancy concentration and frequency (10^2-10^6 Hz) at room temperature. The variation of dielectric constant with frequency indicates dispersive behavior and giant dielectric response

(more than 10^4) at low frequencies for compounds deficient in oxygen. Such value of ε' makes these samples an interesting material to be used in applications namely the reduction of electronic components size. To summarize, incorporating vacancy oxygen enhances the dielectric properties. Thus, the interesting dielectric constant and weak loss strengthen the use for potential applications.

Keywords: Oxygen vacancy, Sol gel method, Optical property, Dielectric constant.

*Corresponding author.

E-mail address: maryemmrc2@gmail.com (M. Bouzayen)

I. Introduction

Conventional perovskites with general formula ABO_3, where A is rare earth and B is a metal transition, play a major role in the development of technological applications **[1, 2]**. These materials are easily prepared, environmentally friendly and show interesting properties **[3, 4]**. Lanthanum orthoferrite, $LaFeO_3$, has been considered as one of the most important and known perovskite thanks to its significant potential in many applications **[5-7]**. $LaFeO_3$ is an antiferromagnetic (AFM) insulator with high Néel temperature (T_N~740°C.) The stoichiometric $LaFeO_3$ oxide crystallizes in the orthorhombic Pbnm space group due to the tilting of the octahedral FeO_6 **[8]**. The $LaFeO_3$ is known especially for its low band gap energy (Eg<3 eV) and for the presence of oxygen deficient sites in its crystal structure. Taking advantage of these attractive properties, this material is used in scientific and technological research fields **[9-14]**.

The cationic substitution into La- sites by lower- valent cations such as Sr^{2+} **[15, 16]**, Ba^{2+} **[17]** and Ca^{2+} **[18]** in $LaFeO_3$ modifies the physical properties and improves their

performance. The double substitution of lanthanum ion with 10% of Barium (Ba) and 15% of strontium (Sr) enhances optical and electrical proprieties [**19]**. The co-doping generates oxygen vacancies which gives these compounds a strong asset to be used.

Currently ferroelectric perovskite with colossal dielectric constant (<1000) are a field of interest. This constant is related to hopping charge carriers. We aim, in this work, to improve this property through the incorporation of oxygen vacancy which is considered the main source of electron.

In previous research **[20, 21]**, their properties can be controlled through classical ways such as the synthesis conditions' variation and the doping with various cations. We herein propose a new method based on creating quantified oxygen vacancies leading to mixed valence of iron ion Fe^{2+}/Fe^{3+}.

This method **[22, 23]** has aroused much attention thanks to the important application of these vacancies in high-temperature electrolysis oxygen sensors and catalysis. Moreover, it opens an opportunity for new multiferroic materials. This process is based on the implantation of oxygen vacancies using pure metallic titanium Ti.

The creation of oxygen vacancies in $La_{0.75}Ba_{0.10}Sr_{0.15}FeO_{3-\delta}$ compounds will change the proportions of Fe states. Fe^{3+} and Fe^{2+} concentrations would change with the amount of δ according to the developmental electronic formula:

$$\boldsymbol{La^{3+}_{0.75}Ba^{2+}_{0.10}Sr^{2+}_{0.15}Fe^{2+}_{2\delta}\,Fe^{3+}_{1-2\delta}O^{2-}_{2.875-\delta}}$$

Where, Fe^{2+} and Fe^{3+} concentrations are (2δ) and (1-2δ), respectively.

In order to examine the influence of oxygen non stoichiometry on physical properties, the present paper is focused on the synthesis and investigation of the structure, surface

morphology , optical and dielectric properties of $La_{0.75}$ $Ba_{0.10}$ $Sr_{0.15}Fe$ $O_{2.875-\delta}$ (δ=0.00, 0.125 and 0.25) compounds.

II. Experimental method and Apparatus

The $La_{0.75}Ba_{0.10}Sr_{0.15}FeO_{2.875-\delta}$ samples, with different oxygen vacancies concentrations (δ=0.00, 0.125 and 0.25), were synthesized following two steps:

- $La_{0.75}Ba_{0.10}Sr_{0.15}FeO_3$ (LBSFO) parent compound was prepared by the sol-gel method. Firstly, lanthanum nitrate $La(NO_3)_3.6H_2O$, barium nitrate $Ba(NO_3)_2$, strontium nitrate $Sr(NO_3)_2$ and ferric nitrate $Fe(NO_3)_3.9H_2O$ with purity up to 99.9% were mixed in distilled water. The mixture was thoroughly stirred by magnetic mixer at 70°C. Then, acid citric ($C_6H_7O_7$) with the amount of: n ($La^{3+}+Ba^{2+}+Sr^{2+}+Fe^{3+}$): n (acid citric) =1:2 was added to the mixture under a magnetic stirring for 1hour. Ethylene glycol (PEG molecular weight 20.000) was added later with molar ratio citric acid: ethylene = 4:10 under constant stirring. The acid citric and ethylene glycol were used as chelating agents to promote polymerization and subsequently gel formation. The obtained gel was heated at 170°C until the formation of black powder which was carefully ground. This powder was fired at 300°C for 12 hours, then it was pressed into pellets forms (of about 5 mm diameter and 1mm thickness). Finally the obtained powder was annealed at 600°C, 800°C, and 900°C for 24h, 48h and 24h, respectively.

It should be noted that the valence state (+4) of iron is metastable and the electronic charge compensation was generated by the formation of oxygen vacancies. The oxygen in LBSFO is not 100% stoichiometric and presents weak oxygen vacancies concentration ($\delta \approx 0.125$) according to following equation:

$$La^{3+}_{0.75}\ Ba^{2+}_{0.1}\ Sr^{2+}_{0.15}\ Fe^{3+}_{0.75}\ Fe^{4+}_{0.25}O^{2-}_{3} \longrightarrow La^{3+}_{0.75}\ Ba^{2+}_{0.1}\ Sr^{2+}_{0.15}\ Fe^{3+}_{1}\ O^{2-}_{3-0.125}$$

(Eq.1)

- The $La_{0.75}\ Ba_{0.10}\ Sr_{0.15}FeO_{2.875-\delta}$ samples were obtained by extracting oxygen from the parental oxide $La_{0.75}\ Ba_{0.10}\ Sr_{0.15}FeO_{2.875}$, that was placed into a quartz tube containing a stoichiometric proportion of metallic titanium as explained in the equation below:

$$\mathbf{La_{0.75}\,Ba_{0.10}\,Sr_{0.15}FeO_{2.875} + \frac{\delta}{2}\,Ti \longrightarrow La_{0.75}\,Ba_{0.10}\,Sr_{0.15}Fe\,O_{2.875-\delta} + \frac{\delta}{2}\,TiO_2}\quad \textbf{(Eq.2)}$$

Where, δ=0.125 and 0.25.

The quartz tube was pumped, sealed and annealed at 800 °C for 21 days.

$La_{0.75}Ba_{0.10}Sr_{0.15}FeO_{2.875-\delta}$ (δ=0.00, 0.125 and 0.25) samples were synthesized by sol-gel method followed by thermally activated process of extracting oxygen. It is clear that the formation of $La_{0.75}Ba_{0.10}Sr_{0.15}FeO_{2.875-\delta}$ composition is mainly caused by high reaction rate with the raw of LBSFO. This kind of reaction is a result of the pure metallic Ti owing high oxygen sorption properties. Under a reducing atmosphere, the Ti picks the oxygen from perovskite phase.

In order to monitor the reaction and determine the real rate of oxygen vacancy created the obtained products were weighted. The rate of oxygen vacancy was checked according to the following equation:

$$\delta = \frac{\Delta m \times M_{mol}}{m \times M_0} \quad \textbf{(Eq.3)}$$

Where,

Δm: Mass difference of the compound before and after the reaction

$M_{mol:}$ Molar mass of the stoichiometric $La_{0.75}Ba_{0.10}Sr_{0.15}FeO_{2.875}$ compound

m: Weight of the used $La_{0.75}Ba_{0.10}Sr_{0.15}FeO_{2.875}$ compound

M_O: Atomic mass of oxygen

We find a good agreement between the δ value obtained and the desired one with an error of 10^{-4}.

The crystal structure of the obtained compounds was checked by X-ray diffraction (XRD) analysis on using CuKα1 radiation (λ= 1.5406A°). The acquisition was in the 2θ range of $20 \leq 2\Theta \leq 80^{\circ}$ with a step of 0.02°. The morphology and composition analysis were carried out using scanning electron microscopy (SEM) equipped with an energy dispersive X-ray system (EDX). The Fourier transform infrared (FTIR) was recorded in the wavenumber range of 3500–500 cm^{-1} using a Perkin Elmer spectrometer to figure out the different vibrational bonds. The optical absorption measurements have been measured from the diffuse reflectance spectroscopy in the wavelength range of 200-800 nm. Concerning the photoluminescence (PL) spectra, they were performed by spectrophotometer with the excitation wavelength of 266 nm. For electric measurements, thin silver was deposited on both sides of pellets with a diameter of 5 mm and thickness 2 mm by evaporation under vacuum through a circular mask.

Results and discussions

1. X-ray characterisation

The room temperature X-ray pattern displayed in **Fig. 1** reveals that all samples show the same pervoskite structure. All peaks are identical and superimposable which can be assigned to the diffraction lines of the orthorhombic $LaFeO_3$ phase (JCPDS file no. 37-1493). One peak corresponding to the secondary phase with low intensities were detected. Their intensity increases with the rise of the δ amount. The structural refinement shows that these peaks matches to Fe_3O_4(space group Fd-3m) phase. The arise of (Fe_3O_4) as impurity phases is generally encountered during the preparation of LFO and its derivates **[24]**.

The inset **Fig. 1** indicates that the principal peak is around 32.25° ;corresponding to the (121) planes. The intensity of the principal peak increases with oxygen vacancies concentrtion δ and the peak is shifted slightly towards lower angles confirming the cell's relaxation, leading to the distortion of FeO_6 octahedra and consequently the increase of the volume.

The Rietveld analysis of the principal phase , using the fullProf program **[25]**, matched the orthorhombic lattice with Pnma space group. **Fig. 2** presents the Rietveld plot of the refinements for the $La_{0.75}Ba_{0.10}Sr_{0.15}FeO_{2.875}$ (LBSFO), $La_{0.75}Ba_{0.10}Sr_{0.15}FeO_{2.75}$ (LBSFO1) and $La_{0.75}Ba_{0.10}Sr_{0.15}FeO_{2.625}$ (LBSFO2) samples. The detailed refinement parameters are gathered in **Table 1**. It is very clear that both orthorhombic lattice parameters and cell volume are proportional to δ vacancy rate. This evolution can have two explanations:

i) According to the electronic formula $La^{3+}_{0.75}Ba^{2+}_{0.10}Sr^{2+}_{0.15}Fe^{2+}_{2\delta}Fe^{3+}_{1-2\delta}O^{2-}_{2.875-\delta}$, the iron ion exists on two valence states. The concentration of Fe^{3+} and Fe^{2+} cations are (1-2δ) and (2δ) respectively. The increase of oxygen vacancies amount favors the reduction of iron ions from Fe^{3+} into Fe^{2+} state with highest ionic radius ($r_{Fe^{3+}} = 0.645Å < r_{Fe^{2+}} = 0.78Å$ **[26]**). This leads to the enhancement of the mean size of cations occupying the B-site $<r_B>$ and as a result the increase of the unit cell volume (The radius of the A-site remains invariant).

The $<r_B>$ value was determined using the following relationship:

$$<r_B> = (1-2\delta)\times r_{Fe^{3+}} + (2\delta)\times r_{Fe^{2+}} \quad \textbf{(Eq. 4)}$$

ii) The reduction of the electrostatic bonding forces between the cations: the oxygen vacancies give rise to repulsive forces between B-sites (cations positively charged). This mainly causes the lattice distortion.

The theoretical X-ray density is obtained using the following equation **[27]**:

$$d_x = \frac{Z \times M}{N_A \times V} \quad \textbf{(Eq. 5)}$$

Where, Z is the molecular number per unit cell (Z=4), M is the molecular weight, N_A is Avegadro number and V the volume of the crystal lattice. The porosity ***P*** was determineted by the formula **[27]**.

$$P(\%) = \left(1 - \frac{d}{d_x}\right) \times 100 \quad \textbf{(Eq. 6)}$$

$$\mathbf{d} = \frac{\mathbf{m}}{\mathbf{V}} \quad \textbf{(Eq. 7)}$$

Where, d is the experimental density and m is the weight. The d_x, d and P are sammurazed in **Table 1**.

It is clear that the oxygen vacancy contributes to the improvement of the porosity which enhances the gaz sensitivity of our ferrites **[28]**. The average crystallite size is estimated from XRD patterns, using the Williamson-Hall and Scherrer method based on the formula below **[29]**:

$$D_S = \frac{K \times \lambda}{\beta \cos\theta} \quad \textbf{(Eq. 8)}$$

Where, D_s is the average crystallite size, K is the shape factor (0.9 for particles of spherical shape), λ is the wavelength used, θ is the angle of the most intense peak (121) and β represents the full width at half maximum of this peak.

As shown, the average crystallite sizes calculated from XRD line broadening D_S are about 32, 41 and 46 nm for LBSFO, LBSFO1 and LBSFO2 respectively, confirming the formation of nanosize compounds.

The Williamson-Hall method is performed to determine the strain and the average crystallite size **[30]**:

$$\beta \times \cos(\theta) = \frac{K \times \lambda}{D_W} + 4 \times \varepsilon \times \sin(\theta) \quad \textbf{(Eq. 9)}$$

Where, D_W is the average crystallite size and ε is the effective strain.

Fig. 3(a), 3(b) and 3(c) show Williamson-Hall plot for LBSFO, LBSFO1 and LBSFO2, respectively. The preferred orientation peaks (020), (121), (220), (240) and (420) are picked to determine the crystallite size and strain. The crystallite size D_W and the strain were extracted from the intercept and the slope of the linear fit data, respectively. The D_S and D_W values are listed in **Table 2**. Mentioning that there is a significant difference between the average crystallite sizes calculated using the sheerer method and the Williamson–Hall one. The equation above illustrates that the line boarding is basically isotropic and the strain is assumed to be uniform in all crystallographic directions. In fact, the Williamson-Hall method is the correction of the Scherrer's formula by taking the strain into account (strain is completely abolished by Scherer method) **[31].**

Morphology characterization

Fig. 4(a), 4(b) and **4(c)** illustrate the scanning electron microscope (SEM) micrographs of $La_{0.75}Ba_{0.10}Sr_{0.15}FeO_{2.875-\delta}$ (δ=0.00, 0.125 and 0.25) and EDX mapping images of each element. The surface morphology of the prepared compounds indicates that most particles have irregular shapes with non-uniform distribution. As can be seen from the micrograph, the existence of large grains with less grains boundary.

In order to examine the distribution of detected elements, EDX mapping of La (Purple),Ba (cyan),Sr (slate blue),Fe (green) and O(red) is checked and presents no uniform dispersion. All samples reveal the presence of characteristic peaks of La, Ba, Sr and Fe elements (the appearance of the Carbone signal can be attributed to carbon tape on which the sample is mounted with holder). The results of EDX analysis are depicted in **Table 3**. The elemental composition values are in a good agreement with the nominal composition (the molar ratio of

about 1:1:3 according to the stoichiometry (La, Ba, Sr)/Fe/O) proving that there is no loss of any integrated element during the sintering.

2. FTIR characterization

The FTIR spectra of $La_{0.75}Ba_{0.10}$ $Sr_{0.15}FeO_{2.875-\delta}$ (δ=0.00, 0.125 and 0.25) in the wavenumber range of 500–3500 cm^{-1} are displayed in **Fig. 5**. All samples feature a very strong band between 583 and 600 cm^{-1}. The strong vibration is typically attributed to the Fe–O stretching vibration characteristics of the group FeO_6 octahedron of the rare earth orthoferrites **[32]**. The Fe-O bands shift slightly in the positions and a significant increase in their intensity has been observed with the increase of δ. These variations are consistent with the peak shift in X-ray diffraction. A small peak around 2162 cm^{-1} can be related to the CO_2 absorption band. Nevertheless, broad and intense absorption bands are observed at 3329, 1707, 1666, 1591, 1460, 1368, 1035 and 859 cm^{-1}, only for the parent compound. The broad band at around 3329 cm^{-1} corresponds to the symmetric and asymmetric stretching vibration of water molecules **[33]**. The absorption bands at 1035 and 859 cm^{-1} can be attributed to the presence of carbonates **[34, 36]**. While the presence of peaks around 1591 and 1460 cm^{-1} confirms the complexation process between citric acid and metal ions and qualifies the asymmetric stretching mode of metal carbonates **[37]**. The peaks at 1707, 1666 and 1368 cm^{-1} are assigned to the C=O, bonding vibrations of the water molecules and nitriles groups, respectively **[38]**.

3. Optical measurements

The aim of the UV-vis absorption and PL measurements is to study the optical photoelectric and electronic properties of semiconductor materials.

Fig. 6 shows the UV–Vis diffusion reflectance analysis of $La_{0.75}Ba_{0.10}Sr_{0.15}FeO_{2.875-\delta}$ (δ=0.00, 0.125 and 0.25) in the wavelengths ranged from 200 to 800 nm. The UV-Visible absorption spectra for all samples point out a sharp and intense absorption band in the visible region (around 300 nm). The absorption coefficient is **[39]**:

$$\alpha = 2.303A/t \quad \textbf{(Eq. 10)}$$

Where, A is the absorbance and t is the thickness of the cuvette 1cm.

It is clear that this coefficient decreases with high wavelengths. According to the literature, this band is ascribed to the electronic transition from the valence band to the conduction band (O 2p → Fe 3d) **[40, 41]**.

The optical band gap value is determined using the Tauc relationship **[42, 43]**:

$$(\alpha \nu h) = A\,(h\nu - E_g)^n \quad \textbf{(Eq. 11)}$$

Where, h is Planck's constant, ν is the photon frequency, Eg is the optical band gap and n is an index that characterizes the optical absorption process.

In previous published work **[44]**, the LaFeO3 compound has a direct band gap. So, theoretically **[45]** n is equal to 1/2 for a direct allowed transition. The Inset of **Fig. 6** displays the variation of $(\alpha h\nu)^2$ vs. photon energy (hν). The optical band gap can be deduced from the tangential line drawn on the linear region of the Tauc plot. The Eg value for δ=0.00, δ=0.125 and δ=0.25 samples is supposed to be equal to 3.25, 4 and 4.1 eV, respectively. The band gap value is found higher in this work due to the small crystallite sizes (about 30 and 40 nm) **[34]**. The samples with δ=0.00, 0.125 and 0.25 have a wide band gap in the visible range indicating that our sample could be a perfect candidate for new high frequency optoelectronic devices **[46]**.

An intense band is detected around 540 nm under 266 nm excitation. We should mention that the emission is detected only for LBSFO1 and LBSFO2 (brick red powder) while LBSFO parental compound is opaque (black powder). **Fig. 7** shows PL spectra of $La_{0.75}Ba_{0.10}Sr_{0.15}FeO_{2.875-\delta}$ (δ= 0.125 and 0.25). The oxygen vacancies creation increases the free electron concentration for LBSFO1 and LBSFO2 samples (check **Eq. 12**). The PL emission was a result of recombination of excited electron- hole pair.

$$O^{2-} \longrightarrow \frac{1}{2} O_2 + V_O^{\bullet\bullet} + 2e^- \quad \textbf{(Eq. 12)}$$

In addition to the Uv-Vis measurement, PL signal can be also attributed to the electronic transitions from the valence band to conduction band **[41]**.

4. Dielectric measurements

Dielectric properties are investigated to understand the conduction process and the origin of dielectric loss. The dielectric permittivity is given by the following relation:

$$\varepsilon^*(\omega) = \varepsilon'(\omega) - j\varepsilon''(\omega) \quad \textbf{(Eq. 13)}$$

Where, $\varepsilon'(\omega)$ and $\varepsilon''(\omega)$ are the real and imaginary parts of dielectric permittivity. The dielectric constant and the dielectric loss can be expressed as follows:

$$\varepsilon' = \frac{(Cp \times t)}{A\,\varepsilon_0} \quad \textbf{(Eq. 14)}$$

$$\varepsilon'' = \frac{t}{\omega A \varepsilon_0 R_p} \quad \textbf{(Eq. 15)}$$

Where, ε_o represents permittivity of free space which is equal to 8.854 x10^{-12} F/m, Cp is the capacitance of the specimen and R is the resistance. A and t are the thickness and the area of the pellet, respectively.

The frequency dependence of the real and imaginary parts of permittivity at room temperature for $La_{0.75}Ba_{0.10}Sr_{0.15}FeO_{2.875}$, $La_{0.75}Ba_{0.10}Sr_{0.15}FeO_{2.75}$ and $La_{0.75}Ba_{0.10}Sr_{0.15}FeO_{2.625}$ samples is given in **Fig. (8)**. As seen, all samples show similar behavior. The sudden decrease of dielectric constant, when frequency increases, indicates the dispersive behavior. Then ε' decreases until it reaches a constant value at higher frequencies. It is remarquable that all samples exhibit very high dielectric constants at low frequencies which may be caused by grains boundary defects, oxygen vacancies… **[47, 48].** The dielectric behavior in these materials can be described through Maxwell–Wagner model **[49, 50]** and explained by Koop's theory of dielectrics **[51]**.

The higher value at low frequencies, according to authors **[52]**, is due to the various origins of polarization: combination of electronic, ionic, dipolar and space charge polarizations.

The obtained giant dielectric constants (exceed than10^4 for LBSFO1) show large polarization of atoms. The hole hopping between Fe^{3+} and Fe^{2+} can be responsible of the dipolar polarization while the oxygen vacancy acts like space charge induced electrical polarization **[53]** in our materials. The creation of oxygen vacancies increases the repulsive Columbic forces between Fe ions. As a result, the elementary dipolar moment increases (increase of FeO_6 tilting).

At low frequencies, the electric dipoles can rotate freely, follow the variation of external field and align themselves with alternating field giving rise to high dielectric constant. As the frequency increases, the dipoles are not moving enough to react with the applied ac electric field and consequently the dielectric constant decreases and remains constant at higher frequencies.

The dielectric constant of sample with δ=0.125 is more than 10^4 (100 time higher than the parental compound one). It is very clear, from the curve, that the increasing of oxygen

vacancy concentration decreases the dielectric constant (2000 for sample with δ=0.25) which is beneficial in for future applications.

The imaginary permittivity ε'' as a variation of frequencies is plotted in **Fig. (8b),** ε''decreases when the frequency increases and remains constant at higher frequencies for all samples. The peak in ε'' is given by the hopping of charge carries Fe^{3+}/Fe^{2+}: This is a common behavior in ferrites **[54]**.

The dielectric loss, defined as the ratio of the imaginary part ε'' and the real partε' , is revealed in **Fig. (8c)**. It can be seen that the variation of tanδ exhibits a very similar behavior as the dielectric constant ε'. At low frequencies, high dielectric loss in the material is noticed which is due to grain boundary defects. Dielectric loss (tgδ) decreases with the increase of oxygen vacancy concentration. The high Dielectric constant and the low dielectric loss are observed after oxygen vacancy creation. That's why these compounds may be suitable to be used in applications such the reduction of electronic components' size **[55]**.

5. Conclusion

In this work, the $La_{0.75}Ba_{0.10}Sr_{0.15}FeO_{2.875-\delta}$ (δ=0.00, 0.125 and 0.25) samples were successfully synthesized by the sol-gel method. The XRD analysis indicates the formation of orthorhombic structure with the detection of a small amount of Fe_3O_4 as secondary phase. The creation of oxygen vacancies leads to a slight increase of both lattice parameters and volume. Besides, the particle size was in nanometric region; between 30 and 40 nm. The optical band gaps increase proportionally to the oxygen vacancy concentration. Regarding the dielectric constant, its plot shows a very high value at low frequency. Such variation can be interpreted by Maxwell-Wagner polarization. The dielectric loss as a function of frequency features the same evolution of ε'.

In summary, the oxygen vacancy improves the dielectric property by performing a very interesting dielectric constant and weak loss which is beneficial for potential applications.

Acknowledgments:

The authors would like to express their appreciation to prof. Dhahri Essebti for his guidance during the preparation. Without his valuable assistance this work would not have been completed.

References

[1] J.W. Yoon, M.L. Grilli, E. Di Bartolomeo, R. Polini, E. Traversa, J. Sens. Actuat. B. Chem. **76** (2001) 483–488.

[2] C. Tofan, D. Klvana, J. Kirchnerova, J. Appl. Catal. B. **36** (2002) 311.

[3] A. S. Bhalla, R. Guo, R. Roy, J. Mater. Res. Innov. **4** (2000) 3.

[4] N. Assoudi, I. Walha, K. Nouri, E. Dhahri, L. Bessais, J. Alloys. Compd. **753** (2018) 282.

[5] G. Martinelli, M.C. Carotta, M. Ferroni, Y. Sadaoka, E. Traversa, J. Sens. Actuat. B. Chem. **24** (1999) 30.

[6] T. M. Rearick, G. L. Catchen, J. M. Adams, J. Phys. Rev. B. **48** (1993) 224.

[7] S. Phokha, S. Pinitsoontorn, S. Rijirawat, S. Maensiri, J. Nanosci. Nanotechnol. **15 (**2015) 9171.

[8] W. C. Koehler, E. O. Wollan, J. Phys. Chem. Solids. **2** (1957) 100.

[9] E.I. Golovenchits, B. D. Laĭkhtman, V. Sanina, JETP. **333** (1980) 223.

[10] D. Kuscer, M. Hrovat, J. Holc, S. Bernik, D. Kolar, J. Power Sources. **61** (1996) 161.

[11] N.N. Toan, S. Saukko, V. Lantto, J. Physica. **327** (2003) 279.

[12] V.V. Kharton, A.P. Viskup, E.N. Naumovich, V.N. Tikhonovich, J. Mater. Res. Bull. **34** (1999) 1311.

[13] K. Huang, H.Y. Lee, J.B. Goodenough, J. Electrochem. Soc. **145** (1999) 3220.

[14] M.H. Hung, M.V.M. Rao, D.S. Tsai, J. Mat. Chem. Phys. **101** (2007) 297.

[15] C.M. Chiu, Y.H. Chang, J. Sens. Actuat. B. Chem. **54** (1999) 236.

[16] C.M. Chiu, Y.H. Chang, J. Thin. Solid. Films. **342** (1999) 15.

[17] L. Sun, H. Qin, K. Wang, M. Zhao, J. Hu, J. Mat. Chem. Phys. **125** (2011) 305.

[18] B.P. Barbero, J.A. Gamboa, L.E. Cadus, J. Appl. Catal. B: Eviron. **65** (2006) 21.

[19] F. B. Abdallah, A. Benali, M. Triki, E. Dhahri, K. Nomenyo, G. Lerondel, J. Mater. Sci: Mater. Electron. **30** (2019) 3349.

[20] M. Lebid, M. Omari, Arab J. Sci. Eng. **39** (2014) 147-152.

[21] Qing Lin, Jianmei Xu, Fang Yang, Xingxing Yang, Yun He, J. Appl. Biomater. Func. Mater. **16** (2018) 17-25.

[22] H. Trabelsi, M. Bejar, E. Dhahri, M.A. Valente, M.P.F. Graça, M. Djermouni, A. Zaoui, J. Magn. Magn. Mater. **478** (2019) 175-186.

[23] W. Hzez, A. Benali, H. Rahmouni, E. Dhahri, K. Khirouni, B.F.O. Costa, J. Phys. Chem. Solids. **117** (2018) 1-12.

[24] A. Benali, M. Bejar, E. Dhahri, M.F.P. Graça, L.C. Costa, J. Alloys. Compd. **653** (2015) 506.

[25] H.M. Rietveld, J. Appl. Crystallogr. **2** (1969) 65.

[26] R.D. Shannon, J. Acta. Crystallogr. **32** (1976) 751.

[27] S. Seto, S. Yamada, K. Suzuki, J. Sol. Energy Mater Sol. Cells. **67** (2001) 167.

[28] N. Rezlescu, P.D. Popa, E. Rezlescu, C. Doroftei, Rom. J. Phys. **53** (2008) 545.

[29] A. Guinier, in: X. Dunod (Ed), Theorie et Technique de la radiocristallographie, thirdedition **14** (1964) 3946.

[30] N.S. Goncalves, J.A. Carvalho, Z.M. Lima, J.M. Sasaki, J. Mater. Lett. **87** (2012) 62.

[31] K.K.S. Rao, B. Tilak, K.C.V. Rajulu, A. Swathi, H. Workineh, J. Alloys. Compd. **509** (2011) 7121.

[32] Barbero BP, Gamboa JA, CadÚs LE, J. Appl. Catal. B-Environ. **65** (2006) 21-30**.**

[33] I. Bhat, S. Husain, W. Khan, S.I. Patil, J. Mater. Res. Bull. **48** (2013) 4506-4512.

[34] A.K. Yadav, R.K. Singh, P. Singh, J. Sens. Actuat. B. Chem. **229** (2016) 25-30.

[35] M. Sivakumar, A. Gedanken, W. Zhong, Y.H. Jiang, Y.W. Du, I. Brukental, D. Bhattacharya, Y. Yeshurun, I. Nowik, J. Mater. Chem. **14** (2004) 764–769.

[36] A.A. Davydov, Wiley, New York. (1990).

[37] K.K. Bhargav, A. Maity, S. Ram, S.B. Majumder, J. Sens. Actuat. B. Chem. **195** (2014) 303–312.

[38] N. Sanpo, J. Wang, C.C. Berndt, J. Aust. Ceram. Soc. **49** (2013) 84–91.

[39] X. Zhang, C. Zhang, R. Xie, B. Guo, H. Hu, G. Ma, J. Alloys. Compd. **701** (2017) 170.

[40] L.A. Marusak, R. Messier, W.B. White, J. Phys. Chem. Solids. **41** (1980) 981.

[41] Li. Kuiying, Wa. Dejun, Wu. Fengqing, Xie. Tengfeng, Li. Tiejen, J. Mater. Chem. Phys. (2000).

[42] J. Tauc, Amorphous and Liquid Semiconductors, Plenum Press, New York, (1974) 171.

[43] E.K. Abdel-Khalek, I. Ibrahim, T.M. Salama, A.M. Elseman, M.M. Mohamed, J. Magn. Magn. Mater. **465** (2018) 309.

[44] S. Phokha, S. Pinitsoontorn, S. Maensiri and S. Rujirawat, J. Sol-Gel Sci Technol. **71** (2014) 333– 341.

[45] T.P. McLean and A.F. Gibson (Ed.), Progress in Semiconductors, New York: J. Wiley & sons, inc. (1960).

[46] K. Takenaka, Y. Sawaki, R. Shiozaki, S. Sugai, J. Phys. Rev. B. **62** (2000) 13864–13867.

[47] Ya-Wen Zhang, Xiao Sun, Gang Xu, Chun-Hua Yan, J. Solid. State. Sci. **6** (2004) 523-531.

[48] Muddassar Naeem, Nazar Abbas Shah, Iftikhar Hussain Gul, Asghari Maqsood, J. Alloys. Compd. **487** (2009) 739- 743.

[49] J.C. Maxwell, Electricity and Magnetism, Oxford University Press, London, (1973).

[50] K.W. Wagner, J. Ann. Phys. **40** (1993) 818-822.

[51] C.G. Koops, J. Phys. Rev. **83** (1951) 121-124.

[52] H. Rahmouni, M. Smari, B. Cherif, E. Dhahri, K. Khirouni, J. Dalton. Trans. **44** (2015) 10457-10466.

[53] S. M. Khetre, H. V. Jadhav, P. N. Jagadale, S. R. Kulal, and S. R. Bamane, J. Adv. Appl. Sci. Res. **2** (2011) 503-511.

[54] S. Manzoor, Sh. Husain, J. Mater. Res. Express. **5** (2018) 55009.

[55] P. Lunkenheimer, V. Bobnar, A. V. Pronin, A. I. Ritus, A. A. Volkov, and A. Loidl, J. Phys. Rev. B. **66** (2002) 052105.

Figure captions:

Fig. 1: X-ray diffraction patterns of $La_{0.75}Ba_{0.10}Sr_{0.15}FeO_{2.875-\delta}$ (δ=0.00, 0.125 and 0.25) compounds. Inset: the variation of the principal peaks of $La_{0.75}Ba_{0.10}Sr_{0.15}FeO_{2.875-\delta}$ (δ=0.00, 0.125 and 0.25) compounds.

Fig. 2: Room temperature rietvield refined powder XRD pattern of $La_{0.75}Ba_{0.10}Sr_{0.15}FeO_{2.875\delta}$ (δ=0.00, 0.125 and 0.25) compounds.

Fig. 3: Williamson–Hall plot of $La_{0.75}Ba_{0.10}Sr_{0.15}FeO_{2875-\delta}$: (a) For LBFSO, (b) for LBSFO1 and (c) for LBSFO2.

Fig. 4: SEM micrographs and corresponding EDS spectra of $La_{0.75}Ba_{0.10}Sr_{0.15}FeO_{2.875-\delta}$ (δ=0.00, 0.125 and 0.25) compounds.

Fig. 5: Ftir spectra of $La_{0.75}Ba_{0.10}Sr_{0.15}FeO_{2.875-\delta}$ (δ=0.00, 0.125 and 0.25) compounds.

Fig. 6: UV-Visible absorbance spectra of $La_{0.75}Ba_{0.10}Sr_{0.15}FeO_{2.875-\delta}$ (δ=0.00, 0.125 and 0.25) compounds. Inset: Plots of $(\alpha h\nu)^2$ vs. photon energy (hν).

Fig. 7: PL spectra of $La_{0.75}Ba_{0.10}Sr_{0.15}FeO_{2.875-\delta}$ (δ=0.125 and 0.25) compounds.

Fig. 8: Variation of (a) real part of permitivity, (b) imaginary part of permitivity and (c) dielectric loss (tanδ) with frequency of $La_{0.75}Ba_{0.10}Sr_{0.15}FeO_{2.875-\delta}$ (δ=0.00, 0.125 and 0.25) compounds.

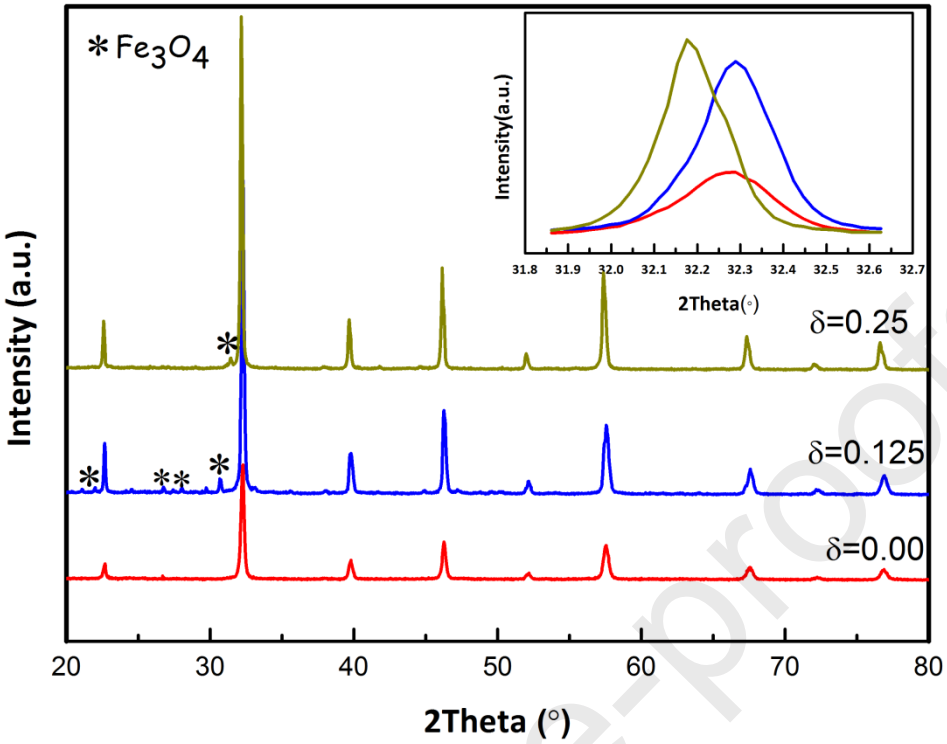

Fig. 1

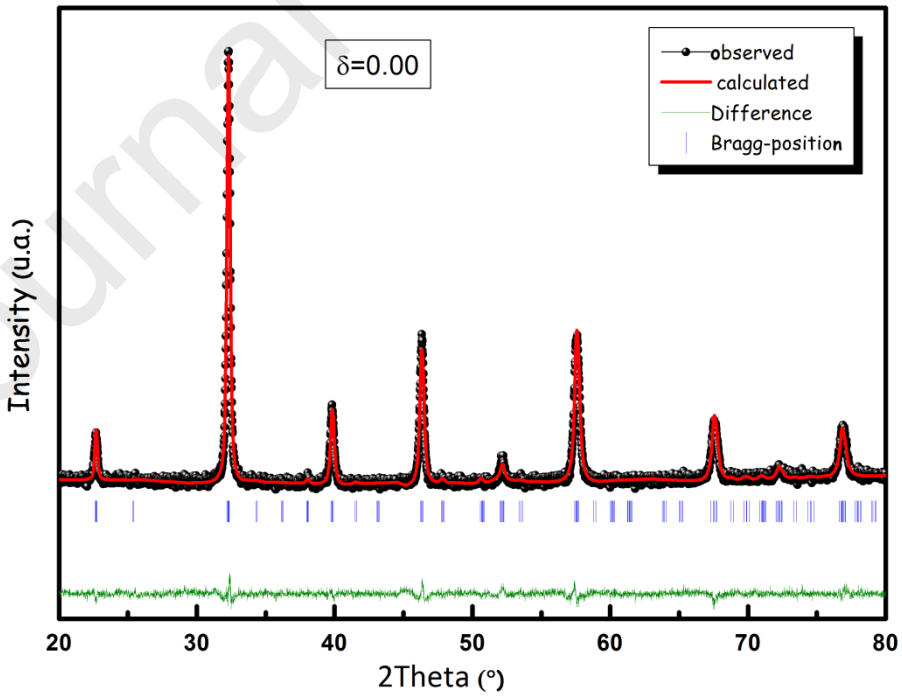

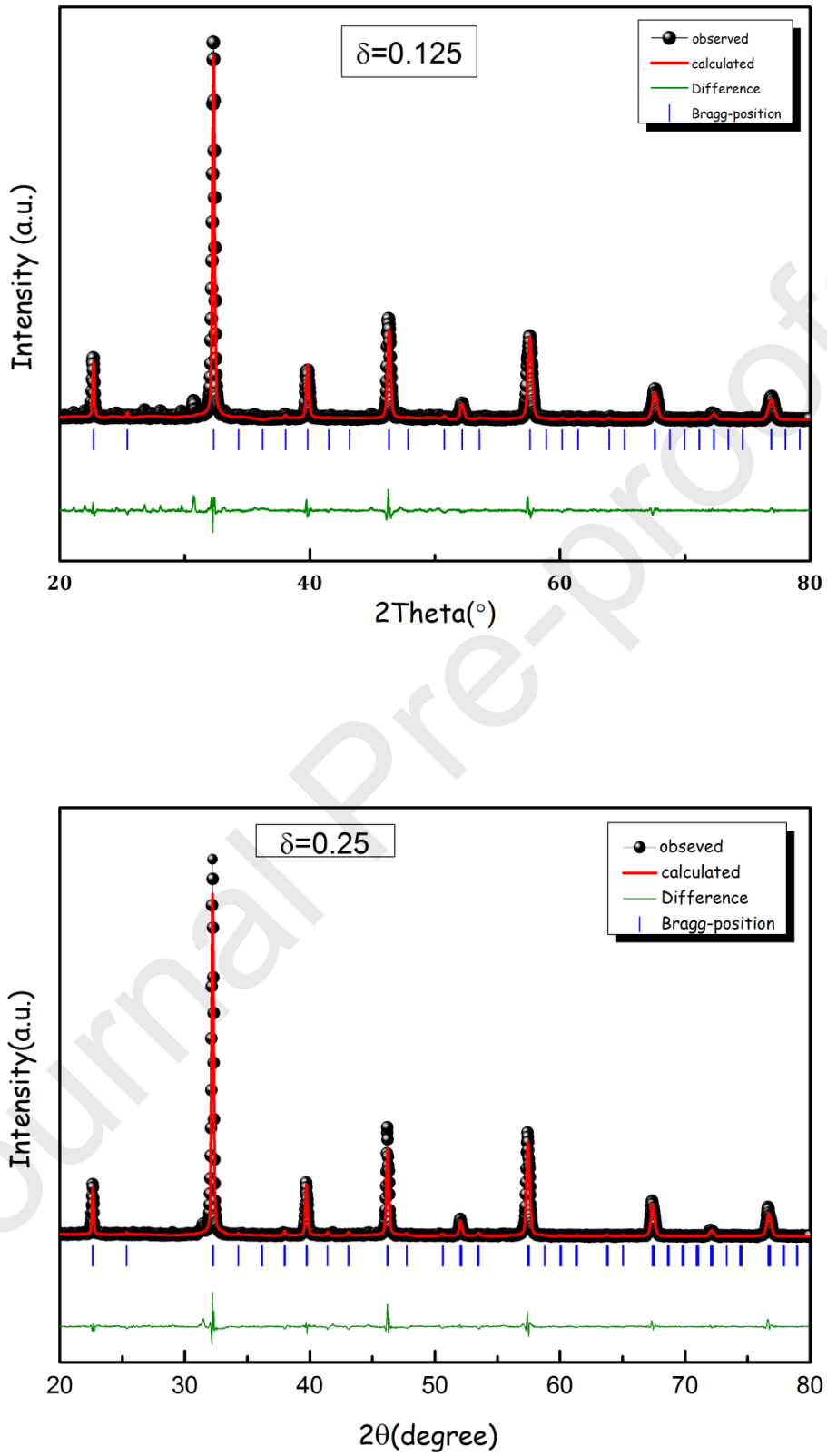

Fig. 2

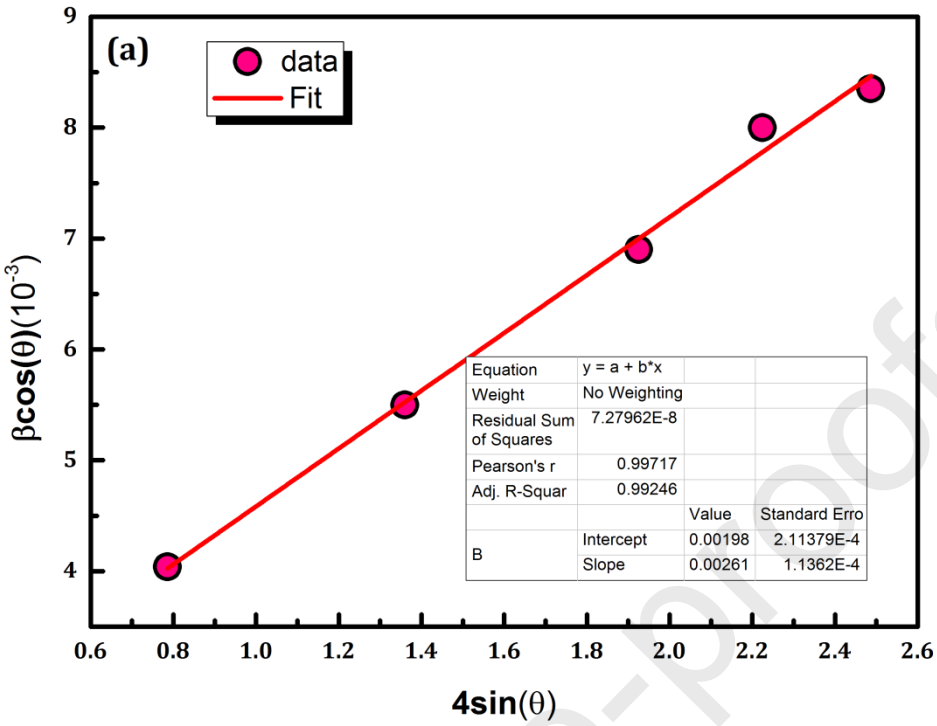

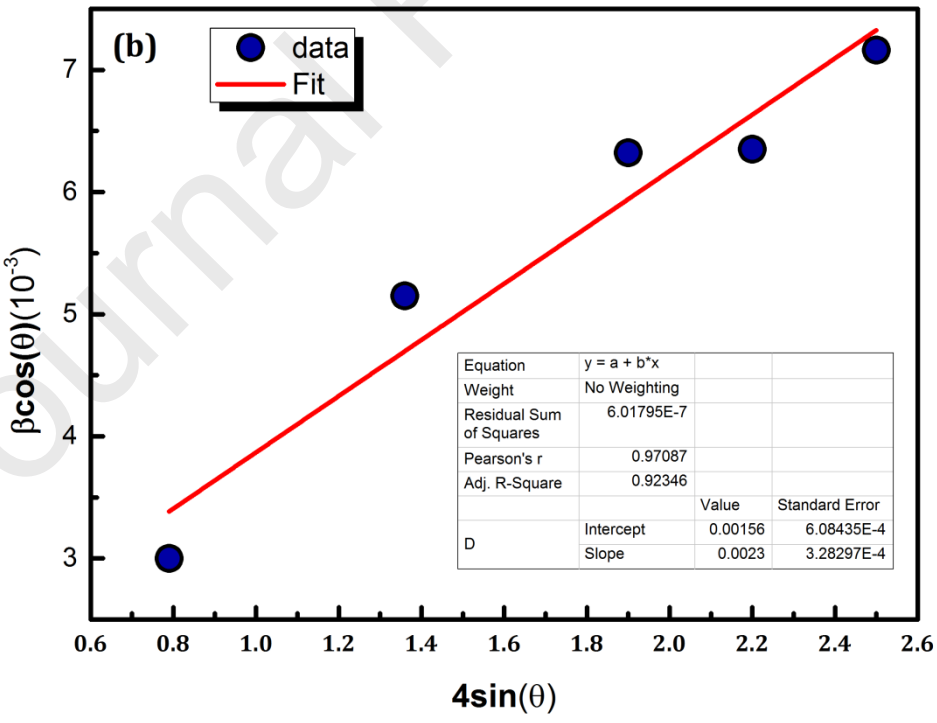

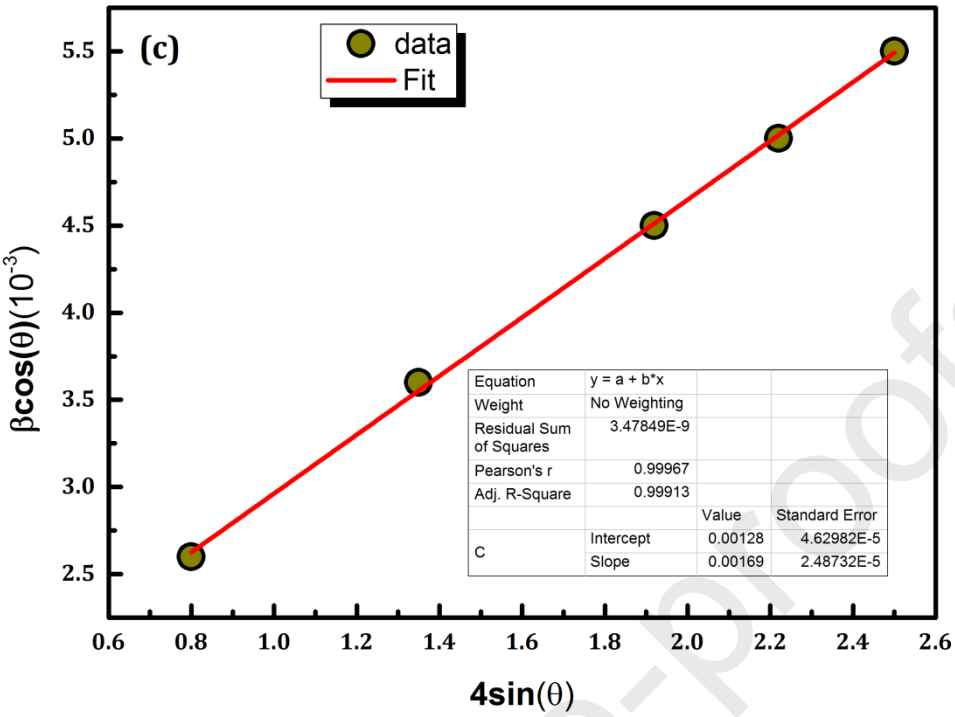
(c)
data
Fit
βcos(θ)(10-3)
4sin(θ)
Equation y = a + b*x
Weight No Weighting
Residual Sum of Squares 3.47849E-9
Pearson's r 0.99967
Adj. R-Square 0.99913
Value Standard Error
C Intercept 0.00128 4.62982E-5
Slope 0.00169 2.48732E-5

Fig. 3

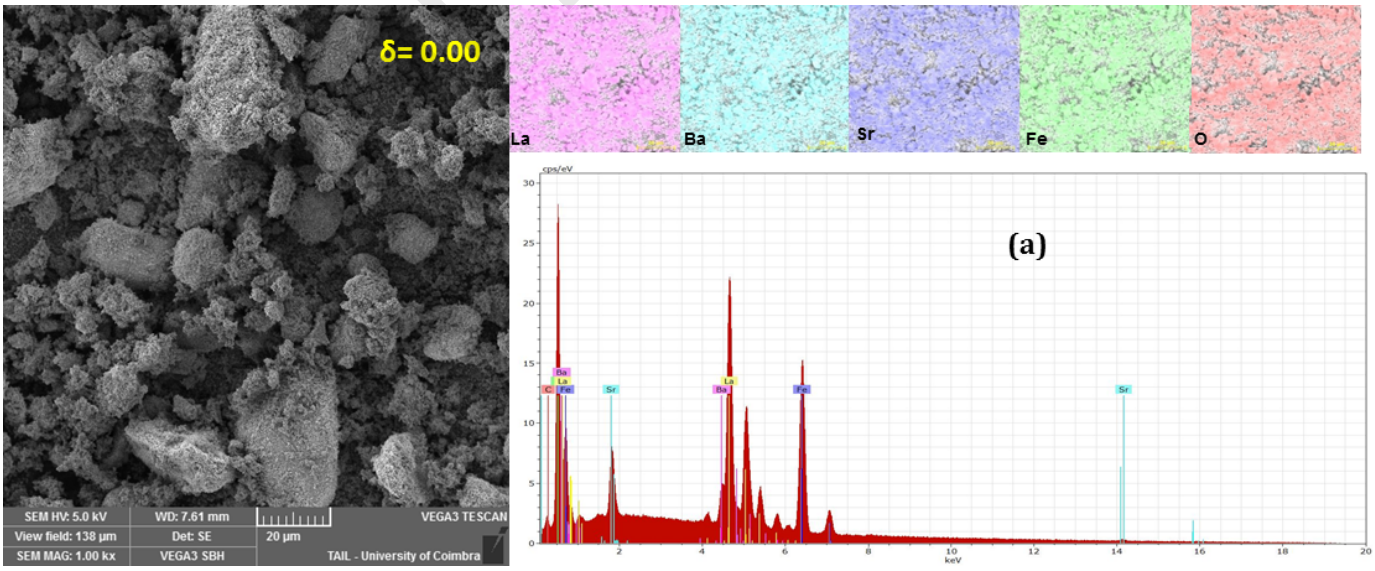
δ= 0.00
La
Ba
Sr
Fe
O
(a)
SEM HV: 5.0 kV
WD: 7.61 mm
VEGA3 TESCAN
View field: 138 µm
Det: SE
20 µm
SEM MAG: 1.00 kx
VEGA3 SBH
TAIL - University of Coimbra

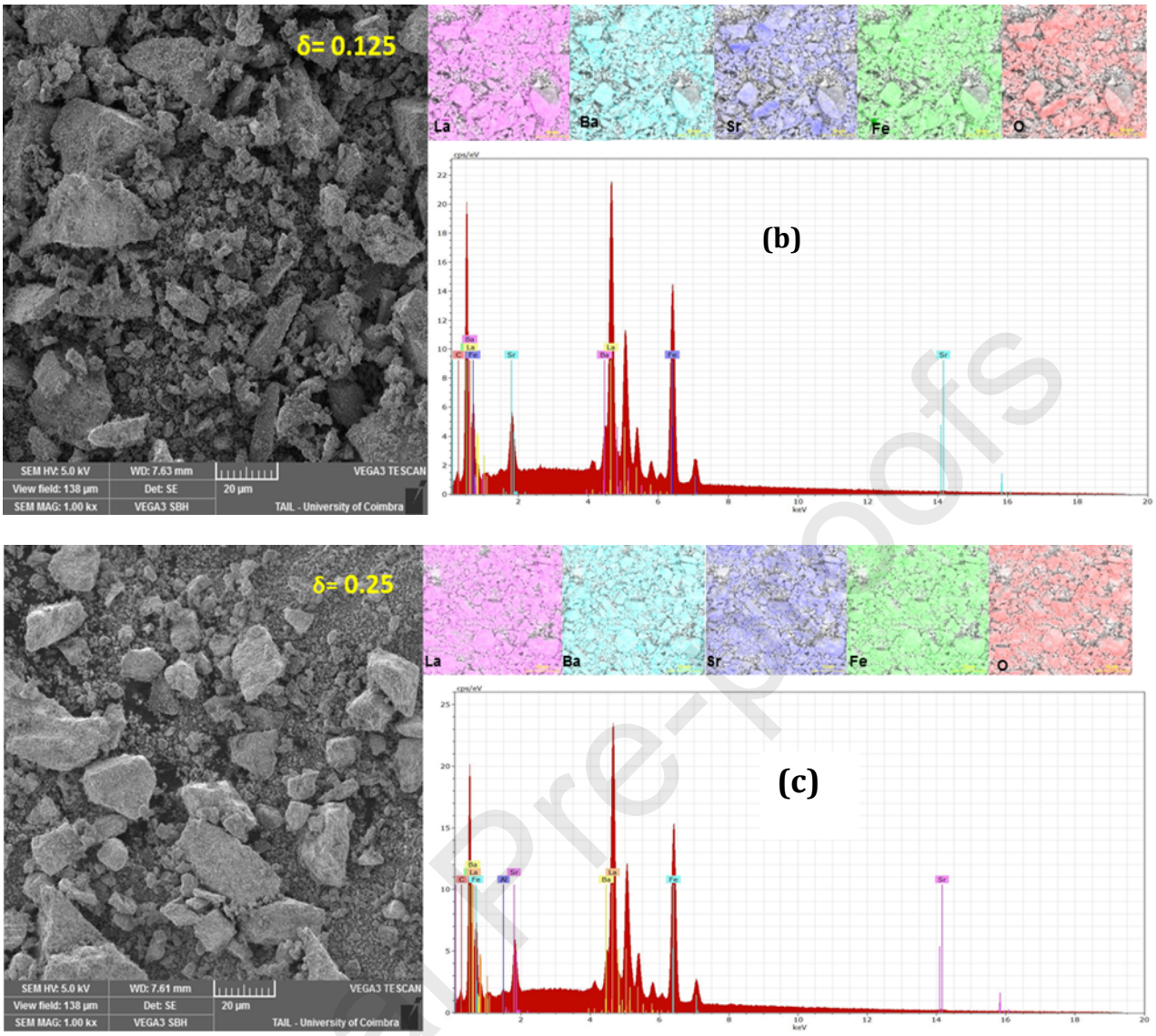

Fig. 4

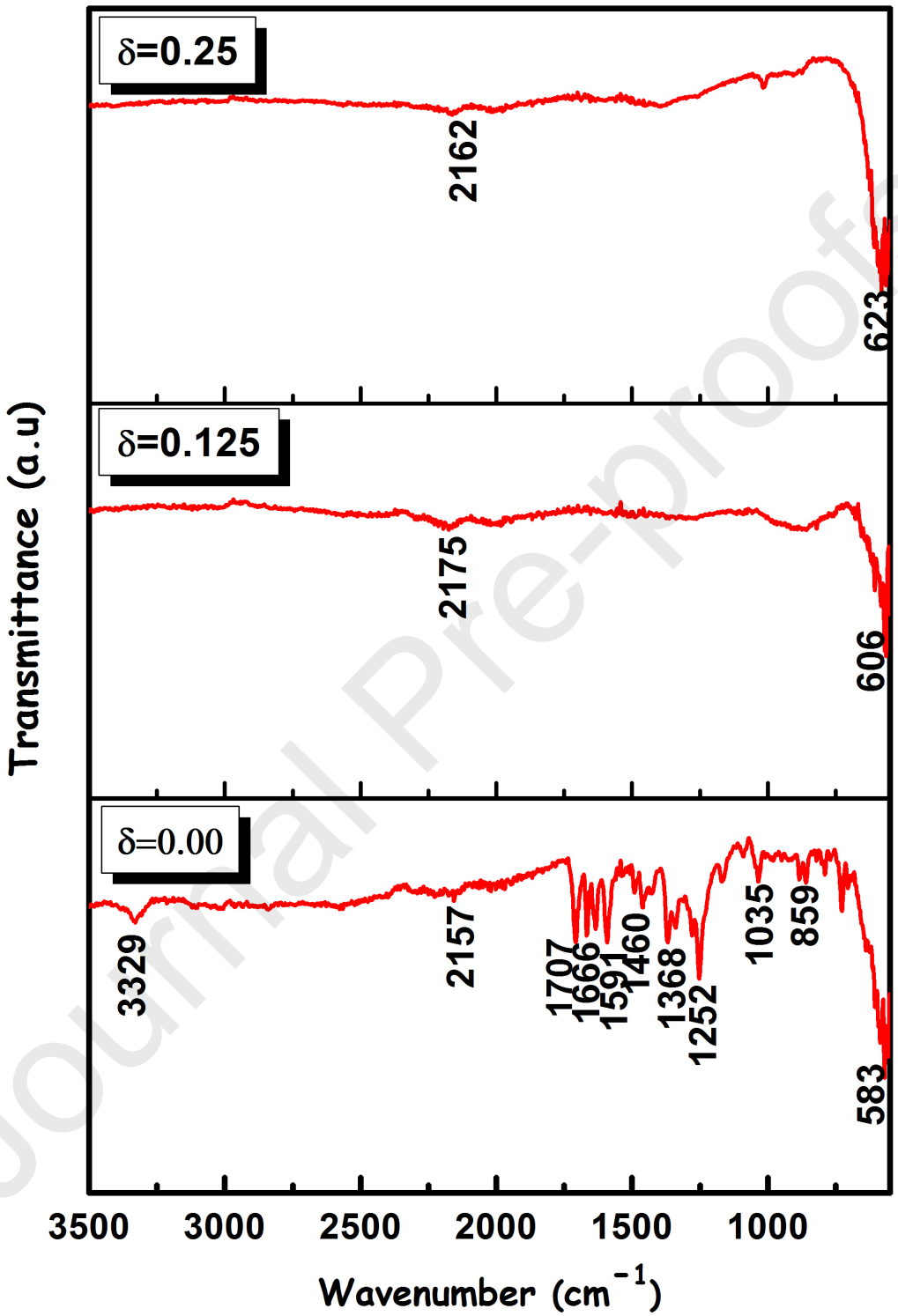

Fig. 5

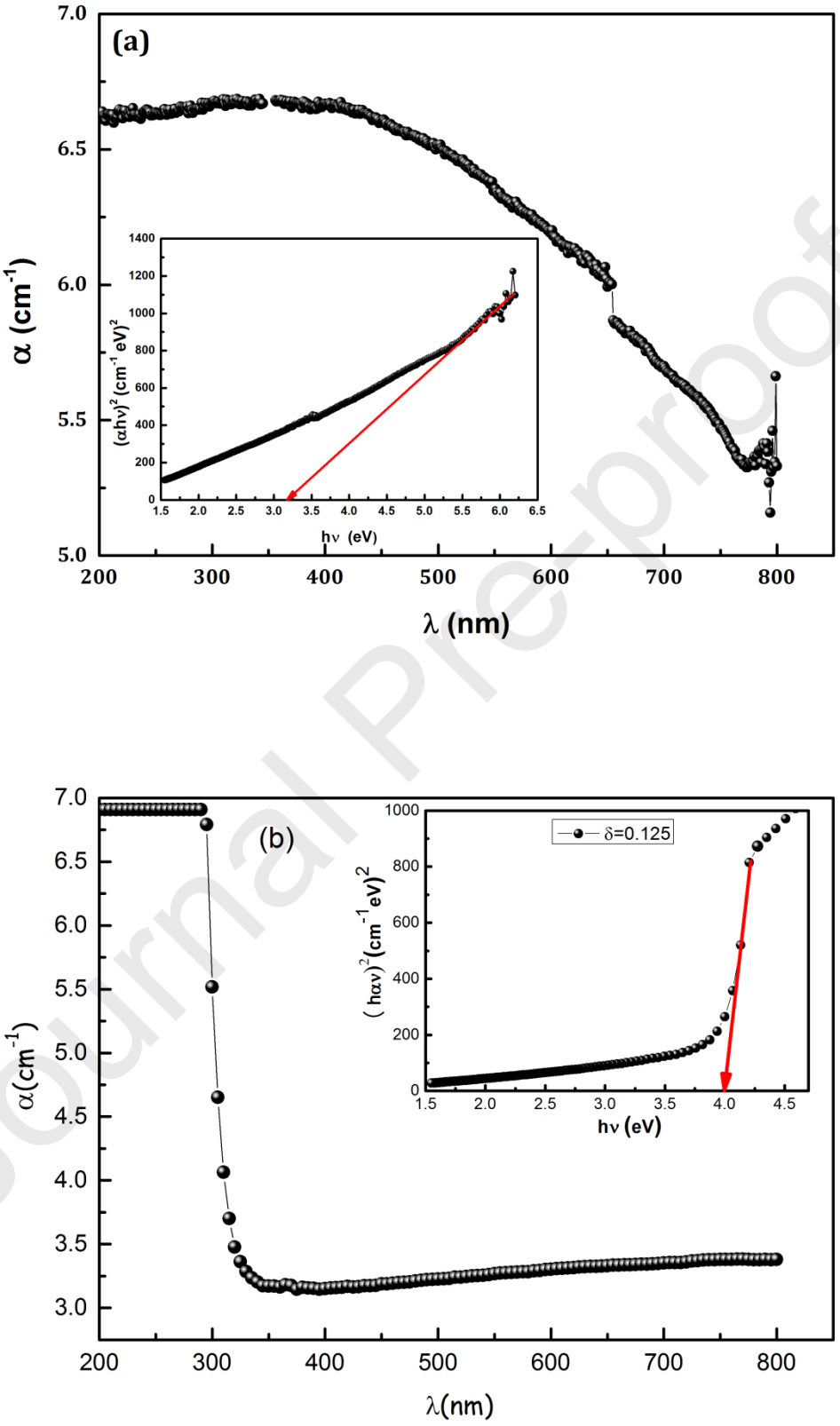

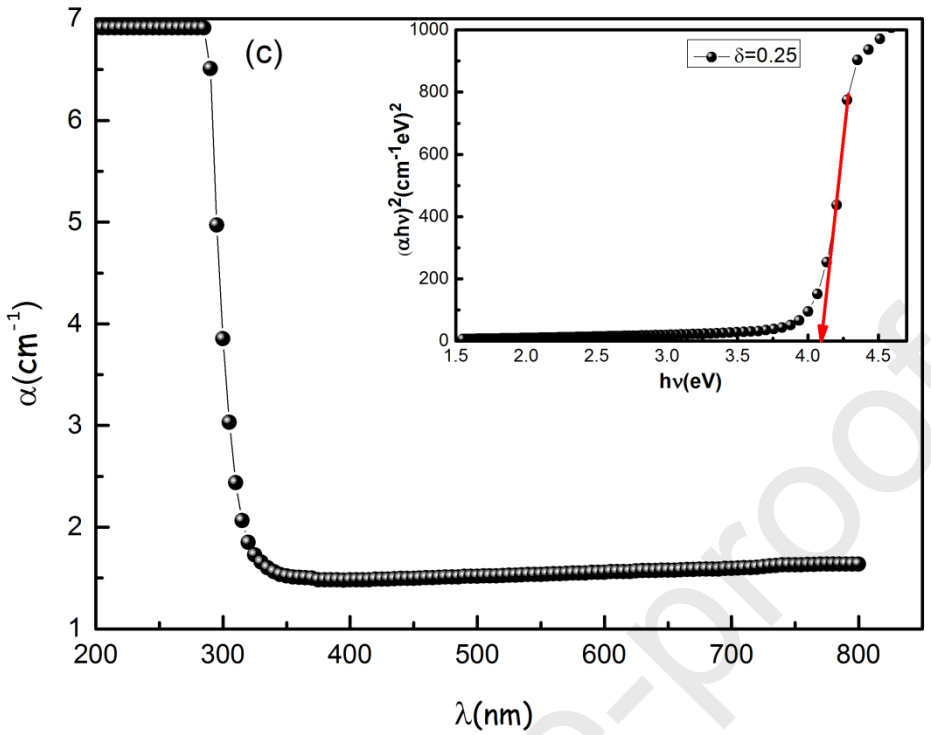

Fig. 6

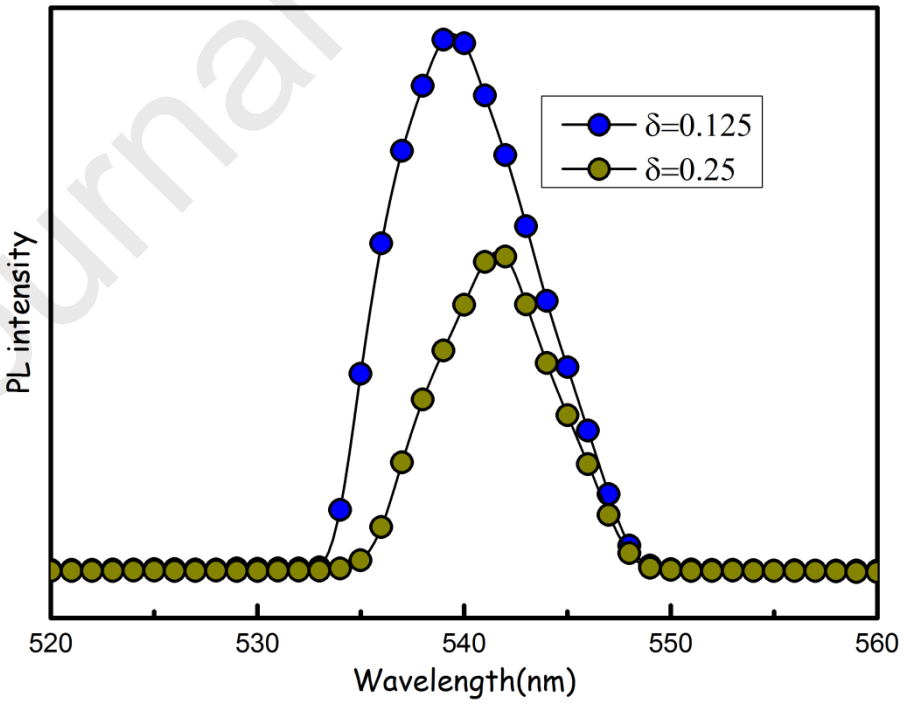

Fig. 7

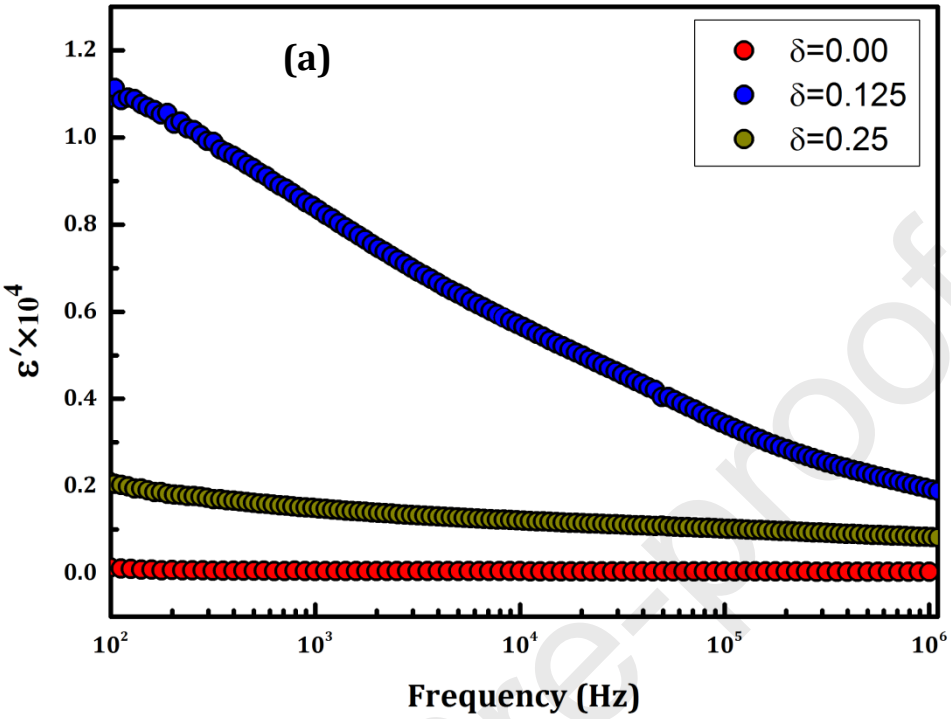

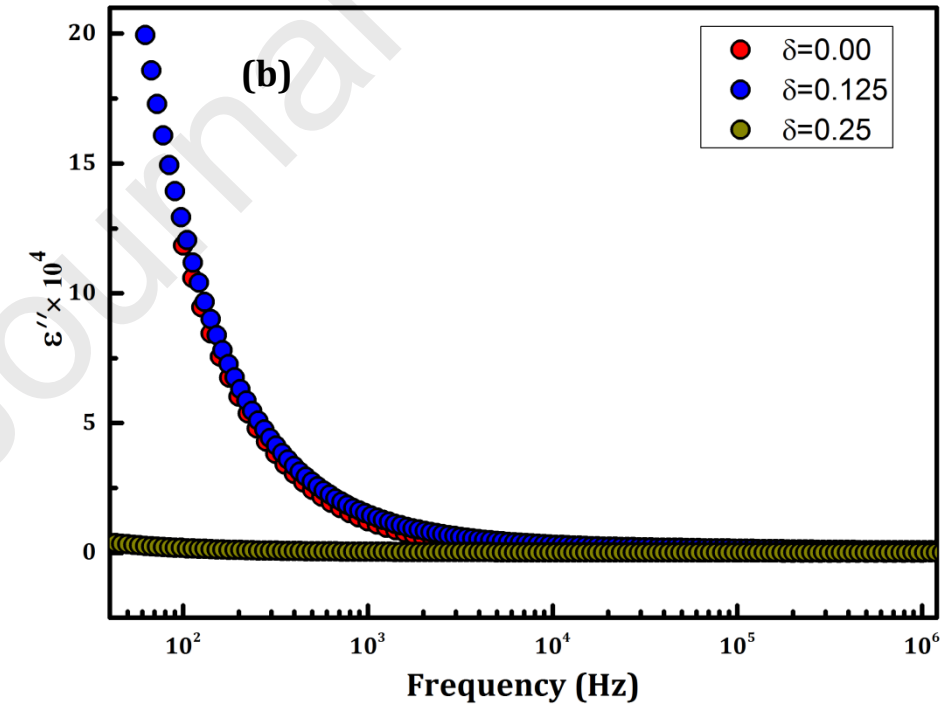

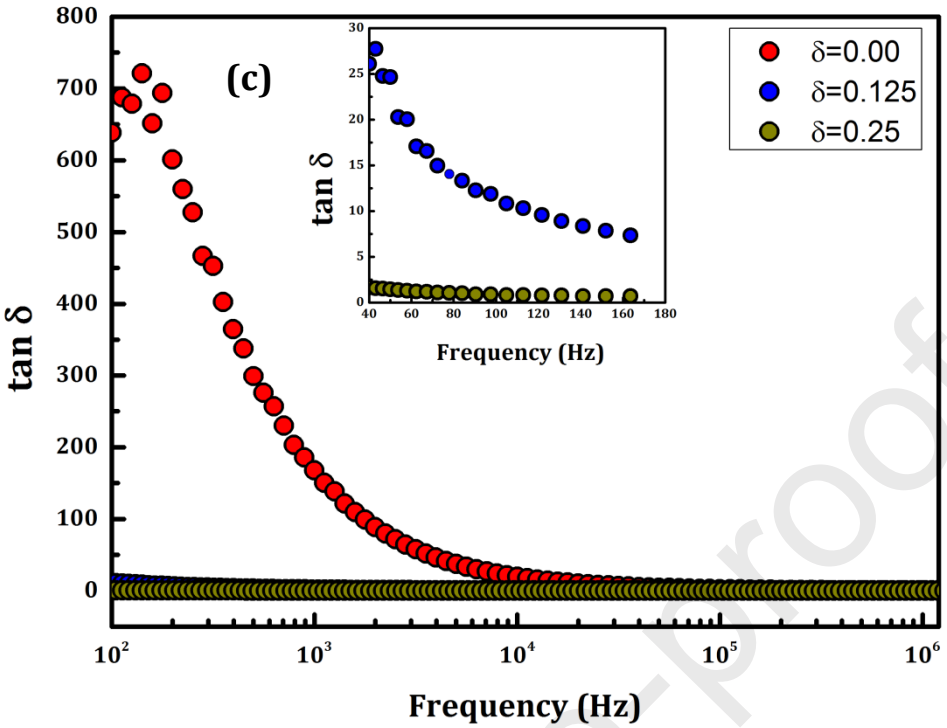

Fig. 8

Research Highlights

- $La_{0.75}Ba_{0.10}Sr_{0.15}FeO_{2.875-\delta}$ (δ=0.00, 0.125 and 0.25) samples prepared by sol gel method followed by thermally activated process
- The three samples crystallize in the orthorhombic structure belonging to Pnma space group, with nanometric crystallite size (30-46 nm)
- For all samples, the FTIR spectra exhibit a very strong vibrational band between 580-620 nm
- Oxygen vacancy creation highly influences the optical and dielectric proprieties
- Compounds owing oxygen vacancy afford important dielectric constant (10^4) and weak loss

Table captions:

Table I: Cell parameters, unit cell volume, mean radii (< r_B>) and X-ray density (d_x) values of $La_{0.75}Ba_{0.10}Sr_{0.15}FeO_{2.875-\delta}$ (δ=0.00, 0.125 and 0.25) samples.

Table II: Average crystallite size values of $La_{0.75}Ba_{0.10}Sr_{0.15}FeO_{2.875-\delta}$ (δ=0.00, 0.125 and 0.25) samples.

Table III: Atomic ratio of element detected of $La_{0.75}Ba_{0.10}Sr_{0.15}FeO_{2.875-\delta}$ (δ=0.00, 0.125 and 0.25) samples.

Table I: Cell parameters and X-ray density values of $La_{0.75}Ba_{0.10}Sr_{0.15}FeO_{2.875-\delta}$ (δ=0.00, 0.125 and 0.25).

δ	0.00	0.125	0.25
Space group	**Pnma**	**Pnma**	**Pnma**
a(Å)	**5.5381**	**5.5397**	**5.5437**
b(Å)	**7.836**	**7.8349**	**7.856**
c(Å)	**5.532**	**5.5435**	**5.5536**
V(Å^3)	**60.129**	**60.151**	**60.467**
<r_B> (Å)	**0.645**	**0.678**	**0.712**
Fe^{2+}(%)	**0**	**25**	**50**
d_x (g/cm^3)	**6.44**	**6.37**	**6.31**
d (g/cm^3)	**4.59**	**4.32**	**3.98**
P (%)	**29**	**32**	**37**

Table II: Average crystallite size values of $La_{0.75}Ba_{0.10}Sr_{0.15}FeO_{2.875-\delta}$ (δ=0.00, 0.125 and 0.15).

Compounds	**Average crystallite size**	
	Scherer's method D_s (nm)	W-H method D_W(nm)
δ= 0.00	32	70
δ= 0.125	41	89
δ = 0.25	46	108

Table III: Atomic ratio of element detected of $La_{0.75}Ba_{0.10}Sr_{0.15}FeO_{2.875-\delta}$ (δ=0.00, 0.125 and 0.25).

Element	**δ=0.00**	**δ=0.125**	**δ= 0.25**
La (%)	10.53	12.91	13.23
Ba (%)	1.70	1.99	2.01
Sr (%)	2.31	2.90	2.78
Fe (%)	15.20	18.02	18.45

Graphical abstract

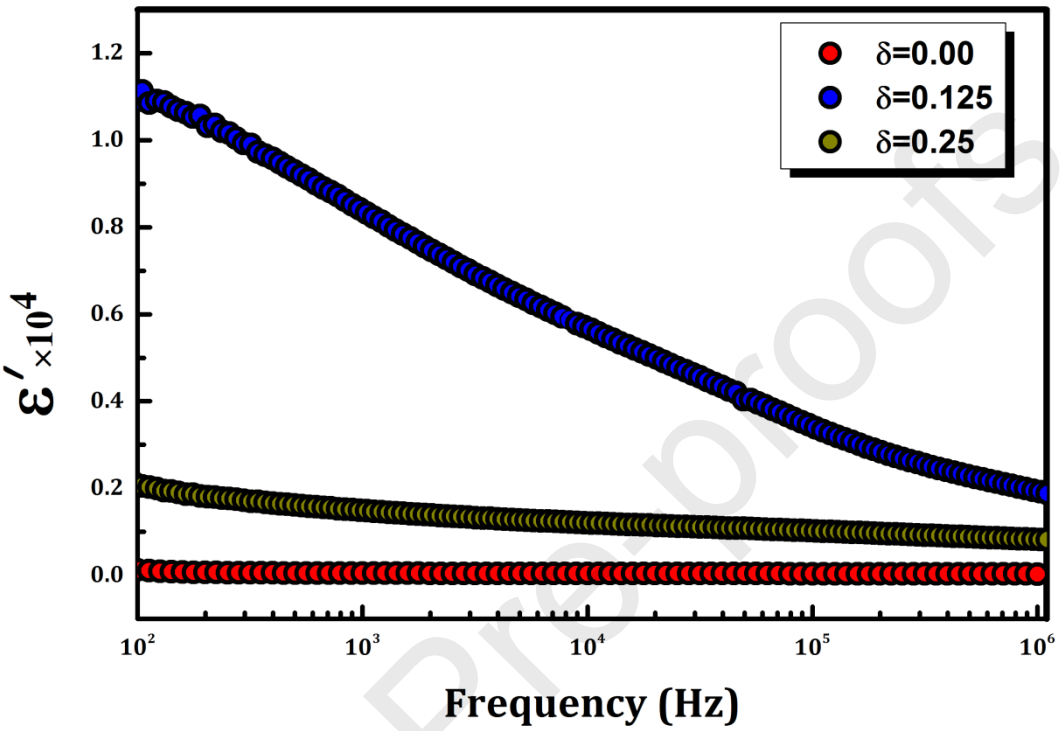

Declaration of interests

☒ The authors declare that they have no known competing financial interests or personal relationships that could have appeared to influence the work reported in this paper.

☐The authors declare the following financial interests/personal relationships which may be considered as potential competing interests:

I declare that they have no known competing financial interests or personal relationships that could have appeared to influence the work reported in this paper

Mariem Bouzayen: Writing- Reviewing and Editing, Writing- Original draft preparation, Radhia Dhahri: Conceptualization, Methodology, Adel Ben ali ,B.F.O Costa and Kamel Khirouni: characterization and investigation ,Salheddine chaabouni : supervision, validation